Environ. Sci. Technol. **1998**, *32,* 3273−3281

Primary Photochemical Reactions in the Photo-Fenton System with Ferric Chloride. 1. A Case Study of Xylidine Oxidation as a Model Compound

V. NADTOCHENKO*

Institute of Chemical Physics Research RAS, Chernogolovka, Moscow District, Russia Federation 142432

J. KIWI*,†

Institute of Physical Chemistry, Swiss Federal Institute of Technology (EPFL) 1015 Lausanne, Switzerland

Environmental contamination in groundwater involving a variety of nonbiodegradable toxic xylidines from industrial or military effluents is a matter of growing concern. Besides the traditional nondestructive treating methods to remove these substances in water bodies, the application of advanced oxidation technologies such as Fenton photoassisted reactions seems a suitable way to remove and mineralize these contaminants and is the aim of the present study. Primary photochemical reactions in the water solutions of ferric chloride complexes in the absence and in the presence of H_2O_2 were examined by laser photolysis ($\lambda = 347$ nm) using xylidine (2,4-dimethylaniline, XYL) as probe molecule. The $Cl_2^{\bullet-}$ radicals are formed as a result of the reaction of $Cl^\bullet$ atoms and $OH^\bullet$ radicals produced during the photodissociation of ferric chloride and ferric hydroxy complexes in the presence of Cl^- anion. The oxidation of xylidine by $Cl^\bullet$ or $Cl_2^{\bullet-}$ lead to the formation of the XYL^+ radical−cation $[C_8H_9NH_2]^{\bullet+}$, having an absorption maximum at $\lambda = 420$ nm which was unambiguously identified by pulsed laser spectroscopy. The decay of XYL^+ radicals in solution takes place within 2 ms in a second-order reaction with $2k = 10^9$ $(M\ s)^{-1}$. In solutions containing $XYL/H_2O_2/FeCl_3$, increasing the oxidant concentration increased the amount of XYL^+, indicating that the H_2O_2 competes with the Cl^- and XYL for the available $Cl^\bullet$ in solution. This was not the case of the anion−radical $Cl_2^{\bullet-}$. To decide if the radical $Cl_2^{\bullet-}$ or $ClOH^{\bullet-}$ prevails after photoexcitation of ferric chloride solutions, a reaction scheme was considered for the formation of the radicals at acidic pH through simultaneous differential equations. The reaction sequence could be kinetically modeled on the basis of laser spectroscopic measurements. The rate constant of $Cl_2^{\bullet-}$ with XYL was found $(3.7 \pm 0.3) \times 10^7$ $(M\ s)^{-1}$. $Cl^\bullet$ atoms oxidize XYL in the reaction with a constant $(4.0 \pm 2.0) \times 10^{10}$ $(M\ s)^{-1}$. The $Cl^\bullet$ atoms react with H_2O_2 with $(1.8 \pm 0.7) \times 10^{10}$ $(M\ s)^{-1}$. The reaction of $Cl^\bullet$ atoms with H_2O_2 explains the decrease observed for $XYL^{\bullet+}$ and $Cl_2^{\bullet-}$ radicals in solution with increasing H_2O_2 concentration. The latter rate constant was observed to be about 5 orders of magnitude higher than the rate constant for the reaction $k(Cl_2^{\bullet-} + H_2O_2 \rightarrow 2Cl^- + H^+ + HO_2^\bullet) = (9.0 \pm 0.4) \times 10^4$ $(M\ s)^{-1}$.

Introduction

Methylanilines (xylidines), which are nonbiodegradable materials that are expensive to treat by nondestructive techniques such as adsorption on activated carbon, are used in a variety of industrial processes in the chemical industry (*1*−*3*). The disposal of fuel rockets (samine) in military bases, active or not, has led in recent years to groundwater contamination by di- and trimethylanilines (*1, 2*). During the course of this study we intend to elucidate the primary and secondary reactions during the photoassisted Fenton degradation of 2,4-dimethylaniline or XYL.

Until now the prevailing general view was that the photo-Fenton reaction (*4, 5*) was synonymous with the photogeneration of $OH^\bullet$ radicals and Fe(II) ions. But recently, photolysis of ferric hydroxy complexes (*6*−*8*) as well as the photolysis of ferric organic complexes $Fe^{III}RCOOH$, $Fe^{III}ROH$ forming Fe(II), and organic radicals has been reported (*9, 10*). In situ production of hydroxy radical $OH^\bullet$ from Fe^{III}/Fe^{II} and H_2O_2 has been reported in dark reactions (*11, 12*).

Ferric chloride is often used in Fenton catalysis (*12*). $FeCl^{2+}$ and $FeCl_2^-$ complexes in solution act as chromophores because they have absorption bands at $\lambda < 400$ nm with maximum close to $\lambda = 340$ nm (*13, 14*). Two different mechanisms have been suggested in the literature for the photodissociation of ferric chloride complexes: (a) The photolysis of complexes with $Cl^\bullet$ atom formation in the presence of organics leading to the chlorination of organic compounds under steady-state illumination (*15*−*17*), and (b) the formation of $Cl^\bullet$ atom due to ferric chloride photodissociation but not leading to chlorinated compounds because the $Cl^\bullet$ yield is negligible (*18*−*20*). The photochemistry of ferric chloride complexes is also important in seawater (*21*). The mechanistic role of ferric chloride complexes in the photoassisted Fenton catalysis has not been reported in detail until now.

This work is designed to provide detailed kinetic data for the photochemistry of iron(III) with Cl^- anion solutions for a better understanding the redox cycling of iron(III)−iron(II) in relation to the photo-Fenton-induced degradation of XYL. Some of the intermediates produced during the photolysis and radiolysis of anilines and xylidines have been reported (*22*−*24*).

Experimental Section

Materials. $FeCl_3 \cdot 6H_2O$, $Fe(ClO_4)_3 \cdot 9H_2O$, $Fe_2(SO_4)_3$ (aq), $LiClO_4$, 2−4 dimethylaniline (XYL), and H_2O_2 were Fluka p.a. and used as received. The solution pH was adjusted with $HClO_4$ or H_2SO_4. In the most experiments the acid corresponding to the counterion in the iron salt was used.

Laser Photolysis and Spectrophotometric Observations. Laser photolysis was carried out by using the second harmonic ($\lambda = 347$ nm) of a JK-2000 ruby laser operated in the Q-switched mode. The pulse width was about 15 ns, and the highest energy per pulse was ∼18 mJ. During the studies the laser pulse energy was monitored and the experimental results normalized accordingly. The mean area of the laser beam was 0.5 cm^2. The detection of the transient absorption changes was performed via an EGG photomultiplier with a rise time of about 5 ns. A detailed account for the laser system has been previously reported (*10*). The preamplifier full bandwidth at 125 MHz was used to register the signals in the nanoseconds up to 2 ms. At longer times the bandwidth was narrowed to 5 MHz. All solutions were used only once to avoid accumulation of the irradiated products. The prevention of the decomposition of XYL was affected in two ways: (a) the solutions were stored in the dark before use and (b) the Xe light beam used for the

* Corresponding authors.

† E-mail: john.kiwi@dcqm.epfl.ch; phone: 41-21-693-3621; fax: 41-21-693-4111.

S0013-936X(97)00962-0 CCC: $15.00
Published on Web 09/10/1998

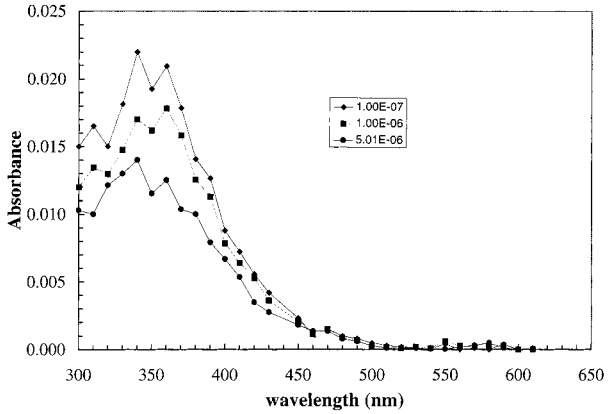

FIGURE 1. Transient absorption spectra of ferric chloride excited complexes as a function of λ. pH = 0.12; [NaCl] = 2 M; [$Fe(ClO_4)_3$] = 0.86 mM.

detection of the intermediates was narrowed by Schott SKF pass band filters. These filters allowed light to come through in a region of $\Delta\lambda$ = 20 nm and were centered at the λ of interest. All experiments were performed in 1-cm quartz cells in aerated solutions at room temperature. Analysis for the absorbance in solutions was carried out by means of a Hewlett-Packard 8452 diode array. The decomposition of the XYL was observed to be negligible when the Fenton reagent was added immediately before taking the spectra.

Results and Discussions

i. Laser Spectroscopy of Fe^{3+} Ions in the Presence of Cl^- Ions in Solution. Figure 1 shows the transient absorption spectra at different times after the laser pulse on Fe^{3+} excited complex species in the presence of Cl^- ions in an aqueous solution. Similar transient absorption spectra were observed for the solution (Figure 1) at different pH values up to a value of pH 2. If iron sulfate was used as a source of Fe^{3+} ions in the presence chloride ions at pH < 2 or $FeCl_3$ is used as Cl^- source, the transient absorption spectra was seen to be close to the results reported in Figure 1. The main feature of this spectra is the strong absorption band increasing up to λ < 450 nm. The spectra of the intermediates shown in Figure 1 suggest a peak at λ = 340 nm for the $Cl_2^{\bullet-}$ radical−anion (*37, 42*). In Figure 1 the peak for this radical−anion is seen to decay at 100 ns after the pulse and continue up to 5 μs. For $Fe(ClO_4)_3$, $FeCl_3$, or iron sulfate solutions, the transient absorption spectra as a function of λ were seen to be independent of the concentration of the salt used and the solution pH up to pH 2.0.

Figure 2 shows the transient absorption spectra for an $FeCl_3$ solution up to the millisecond timeframe. The absorption band up to 2 ms follows the pattern observed for the transient absorption in the microsecond time domain (Figure 1). The inset in Figure 2 shows that bleaching of the transient absorption spectra occurs at λ < 380 nm after ~0.3 ms and extending beyond 3.5 ms. This photobleaching signal is due to the formation of Fe(II) species absorbing less than in the ground state at λ = 380 nm. Due to the make up of the solution used in Figure 2 the long-lived transient signal is ascribed to photoinduced charge separation in agreement with observations by flash photolysis on $FeCl_3$ carried out with longer period of light excitation (*25*).

Figure 3a shows the transients after the laser pulse at λ = 360 nm on a solution of iron perchlorate in the presence of different concentrations of NaCl at pH = 0.8. The ionic strength was adjusted to a value of 2.0 with $LiClO_4$. The transient amplitude is seen to be negligible at zero chloride ion concentration and increases as the NaCl concentration goes up. Figure 3b illustrates the spectrophotometric observations for the same solution. Increasing the NaCl concentration (Figure 3b) had the effect of increasing the absorption at λ = 347 nm. From the similar changes in the transient amplitudes and in the amplitudes of the spectral observations in Figure 3a,b as the concentration of NaCl increases, it is possible to suggest ferric chloride complexes as the photoactive chromophores occurring after the laser pulse.

Figure 4 shows the results for a solution of iron perchlorate after the laser pulse at λ = 360 nm when the NaCl concentration is varied between 0 and 2 M at pH = 2.8. At this pH value a higher concentration of Fe−hydroxy complexes than in the previous experiment (pH < 1.5) is expected. Fe−hydroxy complexes have been reported to photodissociate under light with a formation of $OH^\bullet$ radicals (*6−8, 31−34*). The effect of the $OH^\bullet$ radicals on the transient decay reported in Figure 4. The complexity of the radicals chemistry participation in the reaction sequence is shown in the temporal behavior of the decay transients in Figure 4.

The initial amplitude of the transients is seen to increase when adding NaCl in the 0−1 M range. Surprisingly, a

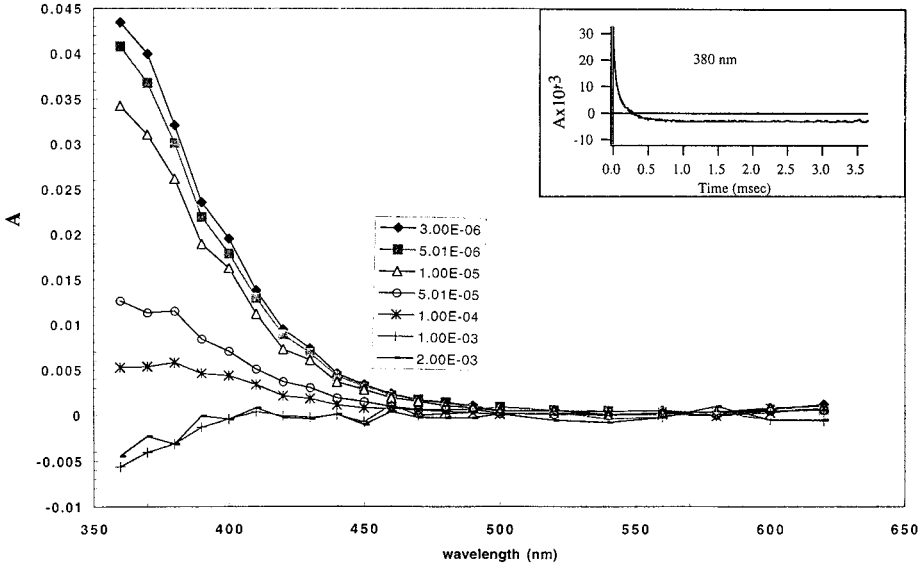

FIGURE 2. Transient absorption spectra after the laser pulse on $FeCl_3$ solutions with a long time domain. [Fe^{3+}] = 0.8 mM at pH 1.56. The inset shows the photobleaching for the transient at λ = 380 nm.

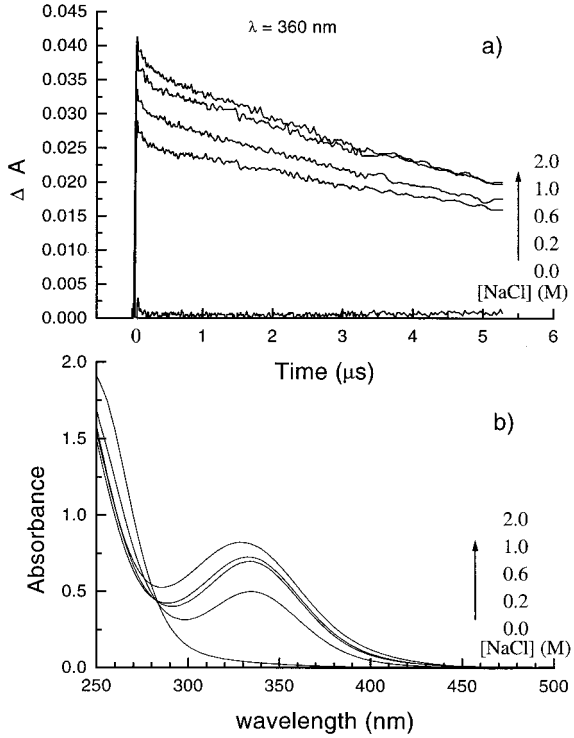

FIGURE 3. (a) Transients in the $Fe(ClO_4)_3$ 0.59 mM solution after the laser pulse registered at $\lambda = 360$ nm at the different NaCl concentrations. pH = 0.8. $LiClO_4$ is used as neutral salt. The ionic strength is 2 for all solutions. (b) Absorption spectra for the $Fe(ClO_4)_3$ 0.59 mM solution at $\lambda = 360$ nm at the different NaCl concentrations at pH 0.8. The ionic strength is 2 for all solutions.

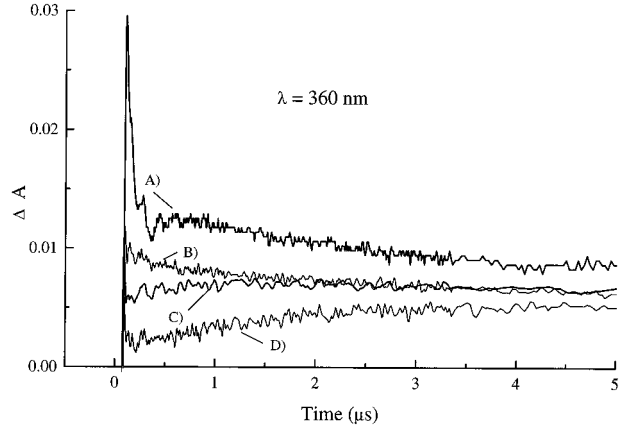

FIGURE 4. Transients in the $Fe(ClO_4)_3$ 0.59 mM solution at $\lambda = 360$ nm at the different NaCl concentrations. pH = 2.8. $LiClO_4$ is used as neutral salt. The ionic strength is 2 for all solutions. Traces: (A) 1.0 M NaCl, (B) 2.0 M NaCl, (C) 0.2 M NaCl, and (D) 0 M NaCl.

marked decrease in the initial amplitude is observed for the transient in the presence of 2 M NaCl. At a low Cl^- anion concentration (<0.2 M NaCl). Figure 4 shows slow kinetics for the signal growth. But at a higher Cl^- anion concentration (>0.2 M NaCl), the transient signals show a decay within 5 μs. Different concentrations of Cl^- in solution produced different amounts of Fe−hydroxy and iron chloride complexes as seen by the transient curves in Figure 4. A quantitative analysis of this system is shown below.

ii. The Nature of Fe^{3+} Complexes in the Presence of Cl^- Ions. The absorption of iron complexes in solutions containing Cl^- ions is a topic of considerable interest (*13, 14, 26−28*). The most important equilibria involving Fe^{3+} ions reactions at acid pH values are shown in Table 1.

TABLE 1. Important Equilibria for Fe^{3+} ions at Acidic pH Values in Aqueous Chloride Solutions[a]

reaction	constant		
$Fe^{3+} + H_2O = FeOH^{2+} + H^+$	K_1	1.9×10^{-3} M^{-1}	(1)
$Fe^{3+} + 2H_2O = Fe(OH)_2^+ + H^+$	K_2	2.5×10^{-9} M^{-2}	(2)
$Fe^{3+} + Cl^- = FeCl^{2+}$	K_3^{Cl}	5.34 M^{-1}	(3)
$Fe^{3+} + 2Cl^- = FeCl_2^+$	K_4^{Cl}	1.82 M^{-2}	(4)

[a] Abbreviations in Table 1: $Fe^{3+} = Fe(H_2O)_6^{3+}$ complex; $FeOH^{2+}$ and $Fe(OH)_2^+ = (H_2O)_5Fe\,OH^{2+}$ and $(H_2O)_4Fe(OH)_2^+$; and $FeCl^{2+}$ and $Fe(Cl)_2^+ = (H_2O)_5FeCl^{2+}$ and $(H_2O)_4Fe(Cl)_2^+$.

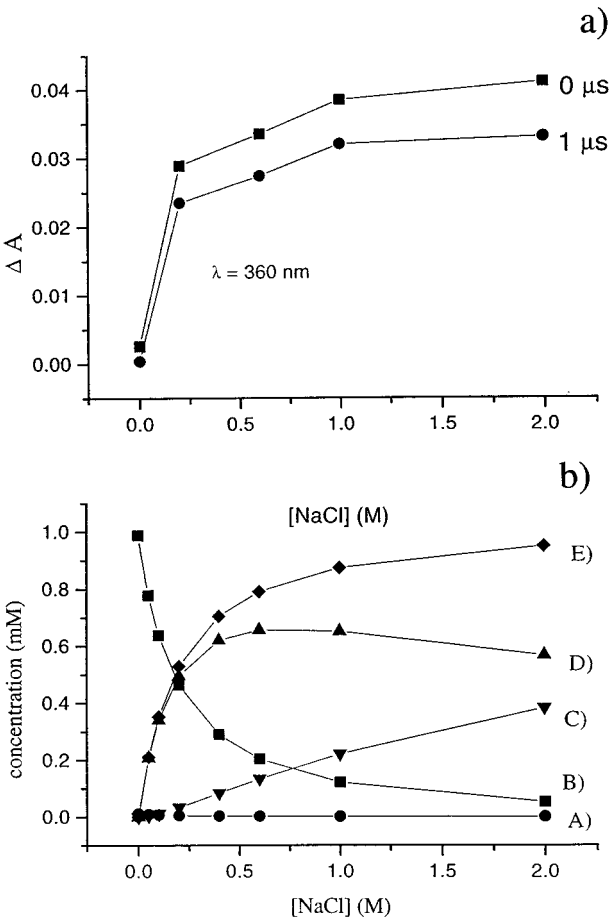

FIGURE 5. (a) The dependence of the transient amplitude after laser pulse as a function of the concentration [NaCl]. Two delay times are presented, 0 and 1 μs. $[Fe(ClO_4)_3] = 0.59$ mM; pH = 0.8; $\lambda = 360$ nm. (b) The dependence of the concentrations of ferric complexes vs [NaCl] at pH = 0.8 calculated according to reactions 1−4: (A) $FeOH^{2+}$, (B) Fe^{3+}, (C) $FeCl_2^+$, (D) $FeCl^{2+}$, and (E) $FeCl_2^+ + FeCl^{2+}$.

The equilibria between ferric ion and its products of hydrolysis are expressed in terms of the formation constants

$$K_1 = \frac{[FeOH^{2+}][H^+]}{[Fe^{3+}]}$$

$$K_2 = \frac{[Fe(OH)_2^+][H^+]^2}{[Fe^{3+}]}$$

which are dependent on temperature and ionic strength. $K_1 = 1.9 \times 10^{-3}$ M, $K_2 = 2.5 \times 10^{-9}$ M^2 at $T = 25$ °C; ionic strength 2 (*13*) the equilibria constants

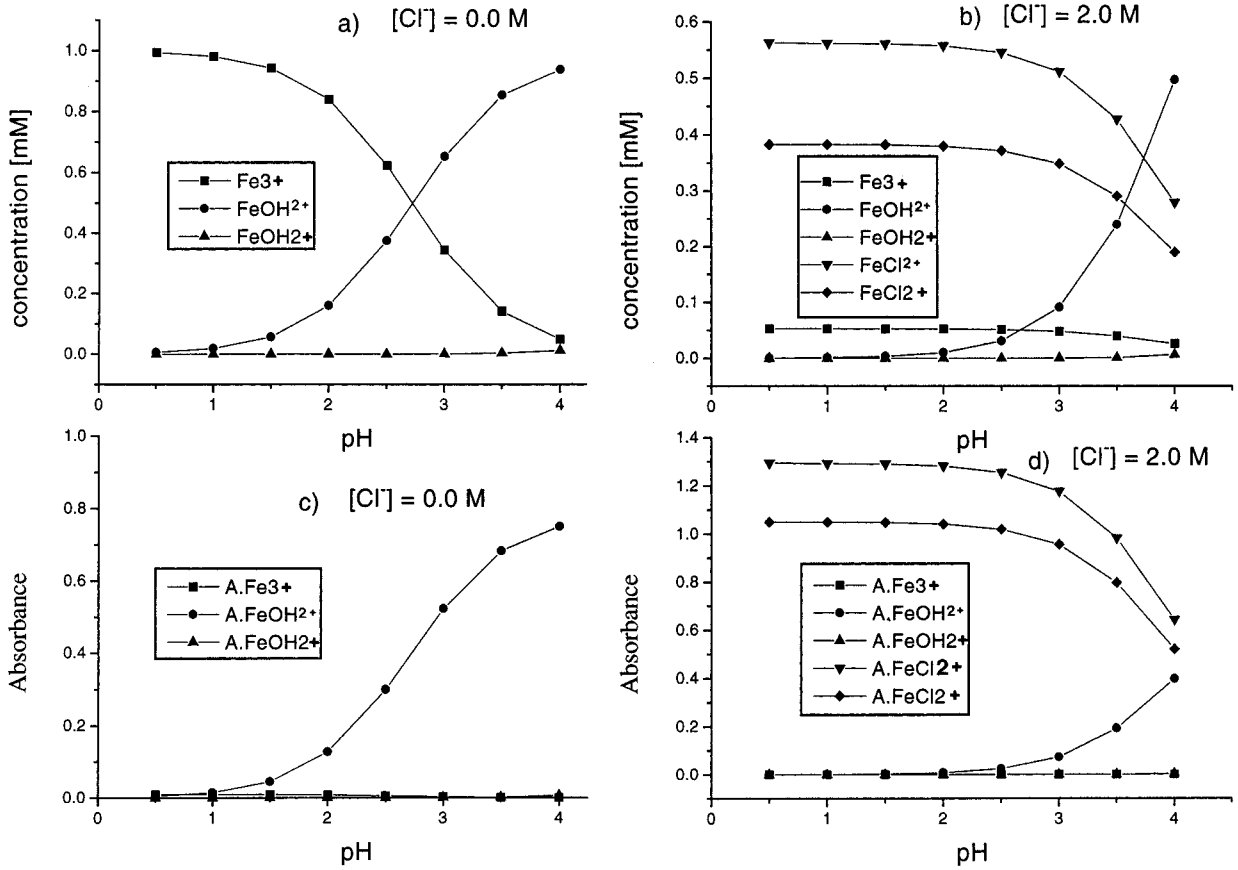

FIGURE 6. The relative concentration of Fe^{3+}, $FeOH^{2+}$, $Fe(OH)_2^{+}$, $FeCl^{2+}$, and $Fe(Cl)_2^{+}$ in the water solution calculated according to eqs 1−4 as a function of the pH. The absorption of the ferric complexes is a function of the pH at a total iron concentration of 1 mM. The Cl^- ion concentration is shown in the figure. For other details see text.

$$K_3^{Cl} = \frac{[FeCl^{2+}]}{[Fe^{3+}][Cl^-]}$$

and

$$K_4^{Cl} = \frac{[Fe(Cl)_2^{+}]}{[Fe^{3+}][Cl^-]^2}$$

are $K_3^{Cl} = 5.34 \times M^{-1}$ and $K_4^{Cl} = 1.82 \times M^{-2}$.

At $\lambda = 347$ nm in the Fe^{3+} species in solution show molar absorption coefficients (*13, 14, 30−34*): $Fe(H_2O)_6^{3+} = 10$ (M cm)$^{-1}$; $Fe(OH)^{2+} = 800$ (M cm)$^{-1}$; $Fe(OH)_2^{+} = 550$ (M cm)$^{-1}$; $FeCl^{2+} = 2300$ (M cm)$^{-1}$; and $Fe(Cl)_2^{+} = 2740$ (M cm)$^{-1}$. The $Fe(H_2O)_6^{3+}$ complex does not absorb light at $\lambda = 347$ nm. The absorption bands of $Fe(OH)^{2+}$, $Fe(OH)_2^{+}$, $FeCl^{2+}$, and $Fe(Cl)_2^{+}$ between 300 and 400 nm correspond to the charge-transfer bands. Usually these bands reflect the shift in charge away from the ligand to the metal center. The formation of the radical species under light proceeds as follows:

$$FeOH^{2+} + h\nu \rightarrow Fe^{2+} + OH^{\bullet} \quad (5)$$

$$FeCl^{2+} + h\nu \rightarrow Fe^{2+} + Cl^{\bullet} \quad (6)$$

$$Fe(OH)_2^{+} + h\nu \rightarrow FeOH^{+} + OH^{\bullet} \quad (7)$$

$$Fe(Cl)_2^{+} + h\nu \rightarrow FeCl^{+} + Cl^{\bullet} \quad (8)$$

Figure 5a presents the dependence of the transient amplitude of the signals previously reported in Figure 3a vs NaCl concentration at two different delay times after the laser pulse. It is possible to plot the relative concentrations of the various Fe^{3+} complexes in solution as a function of NaCl concentration by using eqs 1−4. The results are shown in Figure 5b. From Figure 5a,b, the increase in the amplitude of the transients in Figure 5a occurs in parallel with the increase in the signals observed for the ferric chloride complexes, indicating that these transients are mainly due to photolysis of the latter complexes in solution.

Figure 6 presents the optical absorption and the calculated concentrations of Fe^{3+} hydroxy complexes and Fe^{3+} chloride complexes as a function of solution pH. The iron concentration was 1 mmol in all cases. The concentration profiles shown in Figure 6 were obtained by solving the set of equations corresponding to the equilibria 1−4 for different pH values. As seen from Figure 6a,c, a meaningful absorption of $FeOH^{2+}$ is obtained at a pH < 2 in the absence of the Cl^- ion. Our estimations show that $FeOH^{2+}$ is the main chromophore at 347 nm in the absence of Cl^- ions in solution. In the presence of Cl^- ions (2 M) the laser light is absorbed mostly by $FeCl^{2+}$ and $FeCl^{2+}$ complexes. Only at pH > 1.5 the absorption due to Fe−hydroxy complexes begins to be important. In the presence of Cl^- ions (2 M) the $FeCl^{2+}$ and $FeCl_2^{+}$ in solution were found to be the main absorbing species at $\lambda = 347$ nm (pH < 3). Laser photolysis suggest that $Cl_2^{\bullet-}$ or $ClOH^{\bullet-}$ species are responsible for the transient absorption in Figures 1−5 since these two species absorb in the range 230−450 nm. The $Cl_2^{\bullet-}$ absorption has a maximum at 340 nm with a molar absorption coefficient of 8.8×10^3 (M cm)$^{-1}$. The radical $ClOH^{\bullet-}$ has been reported to have maximum at $\lambda = 350$ nm with a molar absorption coefficient of 3.7×10^3 (M cm)$^{-1}$ (*21−24*). The photodissociation of $FeOH^{2+}$ and $FeCl^{2+}$ occurs under light excitation at $\lambda < 400$ nm (*15−20, 22, 23*). The reactions of $OH^{\bullet}$ radicals with $Cl^{\bullet}$ atoms produce $Cl_2^{\bullet-}$ and $HClO^{\bullet-}$ as reported by radiolysis

TABLE 2. Radical Reactions Involving $Cl^•$, $ClOH^•$, $Cl_2^•$, and $OH^•$ Radicals

reaction	k^+ (forward)	k^- (backward)	
$Cl^• + Cl^- = Cl_2^{•-}$	2×10^{10} $(M\ s)^{-1}$	1.1×10^5 s^{-1}	(9)[a]
$Cl^• + H_2O = ClOH^{•-} + H^+$	1.3×10^3 $(M\ s)^{-1}$	2.1×10^{10} $(M\ s)^{-1}$	(10)[a]
$ClOH^{•-} = OH^• + Cl^-$	6.1×10^9 s^{-1}	4.3×10^9 $(M\ s)^{-1}$	(11)[a]
$Cl^• + Fe^{2+} \rightarrow Cl^- + Fe^{3+}$	5.9×10^9 $(M\ s)^{-1}$		(12)[a]
$Cl_2^{•-} + Fe^{2+} \rightarrow 2Cl^- + Fe^{3+}$	1.4×10^7 $(M\ s)^{-1}$		(13)[a]
$OH^• + Fe^{2+} \rightarrow OH^- + Fe^{3+}$	2.3×10^8 $(M\ s)^{-1}$		(14)[a]
$ClOH^{•-} + Fe^{2+} \rightarrow Cl^- + OH^- + Fe^{3+}$	1.3×10^8 $(M\ s)^{-1}$		(15)[a]
$Cl_2^{•-} + Cl_2^{•-} \rightarrow Cl_3^- + Cl^-$	3.1×10^9 $(M\ s)^{-1}$		(16)[b]
$Cl_3^- = Cl_2 + Cl^-$			
$OH^• + OH^• \rightarrow H_2O_2$	6×10^9 $(M\ s)^{-1}$		(17)[c]

[a–c] Rate constants data from (*a*) ref *37*, (*b*) ref *40*, and (c) ref *12*.

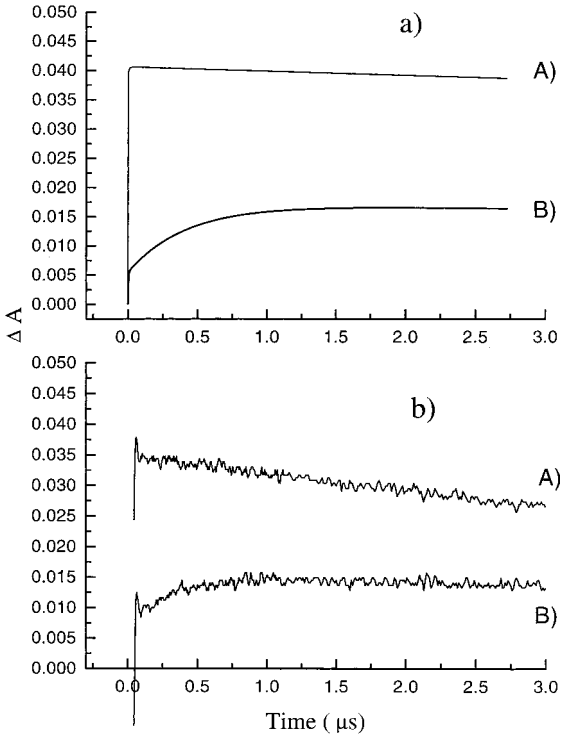

FIGURE 7. (a) The calculated transient curves at $\lambda = 370$ nm. A Runge–Kutta algorithm is used for the solution of the differential equations corresponding to the reactions sequence 9–17. Line A corresponds to the pH = 0.95, and line B corresponds to the pH = 1.92. (b) The experimental transient curves at $\lambda = 370$ nm under the photolysis of solutions: $[FeCl_3] = 0.7$ mM. HCl is used as an acid and as a source of Cl^- anions. Line A corresponds to the pH = 0.95, and line B corresponds to the pH = 1.92.

work (*24–27*). To decide if radical $Cl_2^{•-}$ or $ClOH^{•-}$ prevails after photoexcitation in ferric chloride solutions, the complete scheme shown in Table 2 should be considered for the formation of radicals in solution.

Figure 7a presents the calculated transient curves for the absorption of solutions at $\lambda = 370$ nm. The system of differential equations involving the equations in Table 2 was solved by way of the Runge–Kutta algorithm. Figure 7b shows the transient results obtained by laser photolysis of an $FeCl_3$ solution at different pH's and for different Cl^- anion concentrations. The calculated transients were obtained by the Runge–Kutta algorithm applied to reactions 9–17 using the rate constants in Table 2. The calculated optical density

$$\Delta^{A(t)} = \epsilon_{Cl^-_2}[Cl_2^{•-}](t) + \epsilon_{ClOH^-}[ClOH^{•-}](t) \qquad (18)$$

with the radical concentrations $[Cl_2^{•-}](t)$ and $[ClOH^{•-}](t)$ and $\epsilon_{Cl_2^{•-}}$ and ϵ_{ClOH^-} the molar absorption coefficients at $\lambda = 370$ nm for the two species with values: 8×10^3 $(M\ cm)^{-1}$ and 3×10^3 $(M\ cm)^{-1}$. The initial concentration of the radicals $[Cl^•] + [OH^•]$ was assumed to be 5×10^{-6} M. This last estimation is based on the transient signal observed for $Cl^•$, the molar absorption coefficients of $FeCl_3$, the bleaching of $FeOH^{2+}$ at the concentrations detected in the optical pathlength of the laser beam. The concentrations of ferric complexes Fe^{3+}, $FeOH^{2+}$, $Fe(OH)_2^+$, $FeCl^{2+}$, $Fe(Cl)_2^+$, and Cl^- anions were calculated by algebraic equations the equilibria 1–4. The main feature of Figure 7b was the slow decay of the optical density at the pH = 0.95 and the rise of the transient observed at a pH = 1.92 within 5 μs. The comparison of calculated and measured transients in Figure 7a,b suggests that the scheme of the reactions in the Table 2 adequately interprets the experimental results obtained. The qualitative difference between the transients at pH = 0.95 and pH = 1.92 is explained by the fact that at pH = 0.95 and $[Cl^-] = 114$ mM the radicals $Cl^•$, $OH^•$, $ClOH^{•-}$ are transformed into $Cl_2^{•-}$ in less than 10 ns. At pH = 1.92 and $[Cl^-] = 14$ mM the $OH^•$ and $Cl^•$ render $ClOH^{•-}$ and $Cl_2^{•-}$ formation slower than shown in the transient 2 (Figure 7b). According to the our calculations, the $ClOH^{•-}$ radical concentration is low (10^{-8} M) at both pH = 0.95 and pH = 1.92. The observed transients are attributed to the $Cl_2^{•-}$ absorption less the absorption originating from the photolised ferric complexes.

From the previous considerations the complex shape of the transients in Figure 4a becomes clear. The observed curves are a result of the photolysis of the different ferric complexes $FeOH^{2+}$ and $FeCl^{2+}$. The $OH^•$ radical reacts with the Cl^- anions producing $ClOH^{•-}$ radicals at slower rate as less Cl^- anions exist in solution (*11*). $ClOH^{•-}$ radicals are transformed into $Cl_2^{•-}$ radicals rather fast at low pH due to the reactions 9 and 10. The transient curves in Figure 4 vary as a function of the Cl^- anion concentration. The formation of multicenter ferric complexes has been reported at acidic pH values (*26*). The estimation of the $Fe_2(OH)_2^{4+}$ concentration using the equilibrium constant $K_{eq} = 8 \times 10^{-4}$ M (*42*) shows that there is less than 5% concentration of $FeOH^{2+}$ in this complex form in solution and that this complex is not important in the overall reaction scheme taking place.

The observed bleaching (Figure 2) corresponds to the transformation of the colored ferric chloride complexes into the ferrous uncolored complexes due to the photolysis reactions 5 and 6. The radical decay in the system was determined by the set of reactions 12–17 in which the Fe(II) species is involved. The rate constants of the $OH^•$ radicals recombination (17) and $Cl_2^{•-}$ dismutation (16) are about 1 or 2 orders of magnitude higher than the rate constants of these radicals with Fe(II). The radical decay occurs mostly due to the reactions 15 and 16. For this reason the photogenerated Fe(II) species in solution does not recover to the ferric form completely in the reactions 13 and 14 when reacting with $Cl_2^{•-}$ or $OH^•$ radicals. This is at the origin of

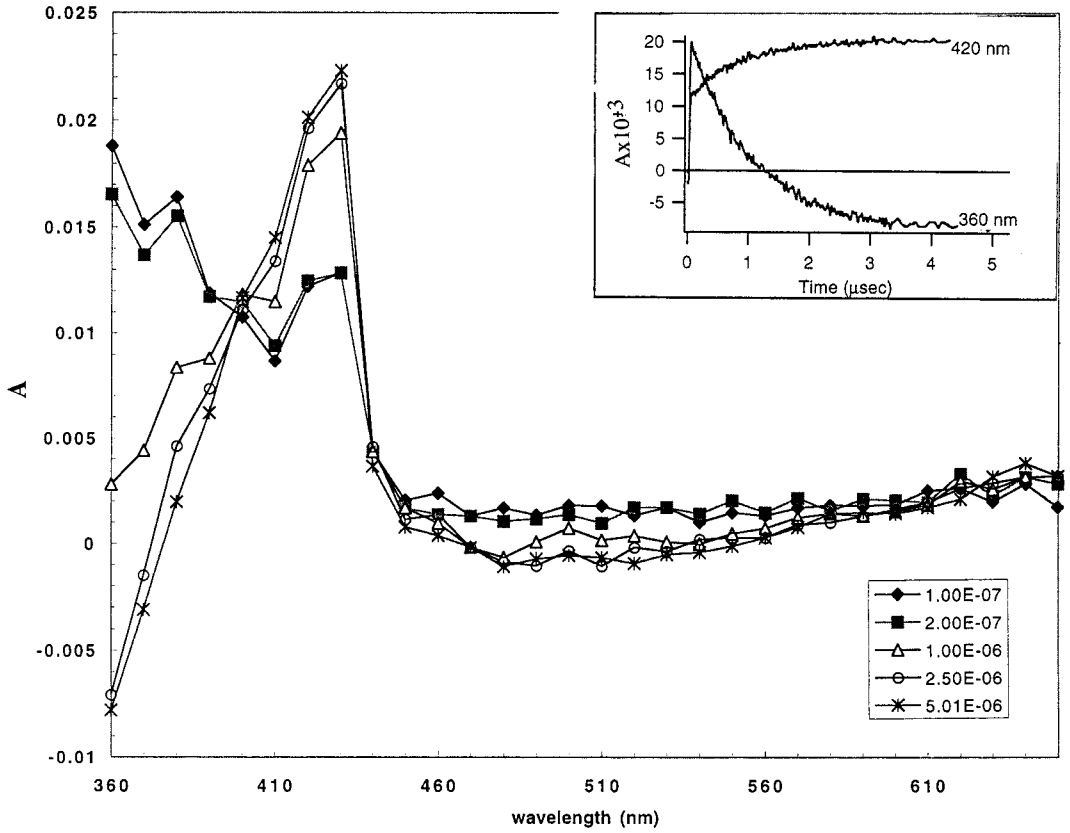

FIGURE 8. Transient absorption spectra after the laser pulse on $FeCl_3$+XYL in solution with a short time domain. [XYL] = 12 mM; [Fe^{3+}] = 1.2 mM at pH 1.6. The inset shows the transients for this system at 420 and 360 nm.

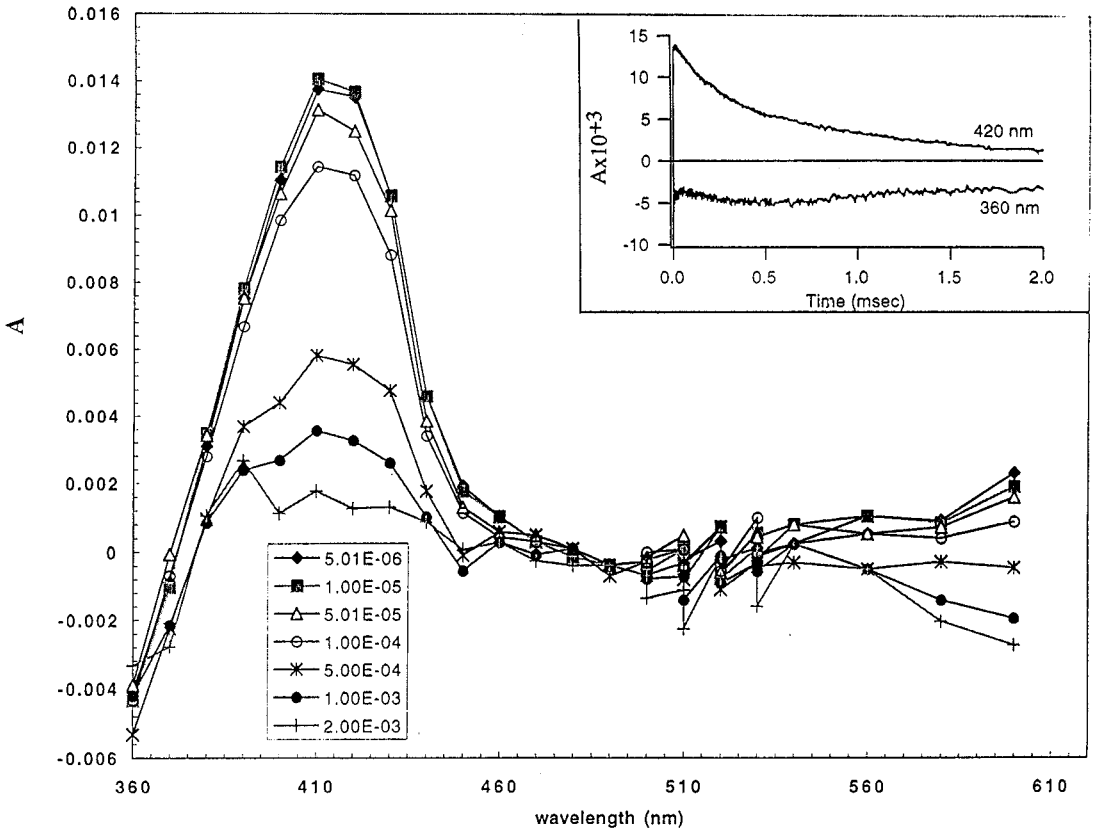

FIGURE 9. Transient absorption spectra after the laser pulse on $FeCl_3$+XYL in solution with a long time domain. [XYL] = 12 mM; [Fe^{3+}] = 1.2 mM at pH 1.6. The inset shows the transients for the system at 420 and 360 nm.

the bleaching observed in Figure 2. The lifetime of $Cl_2^{\bullet-}$ determined from the transient shown in the Figure 7b is about 120 μs. The initial $Cl_2^{\bullet-}$ concentration estimated from the initial optical density of the transient is about (3−5) ×

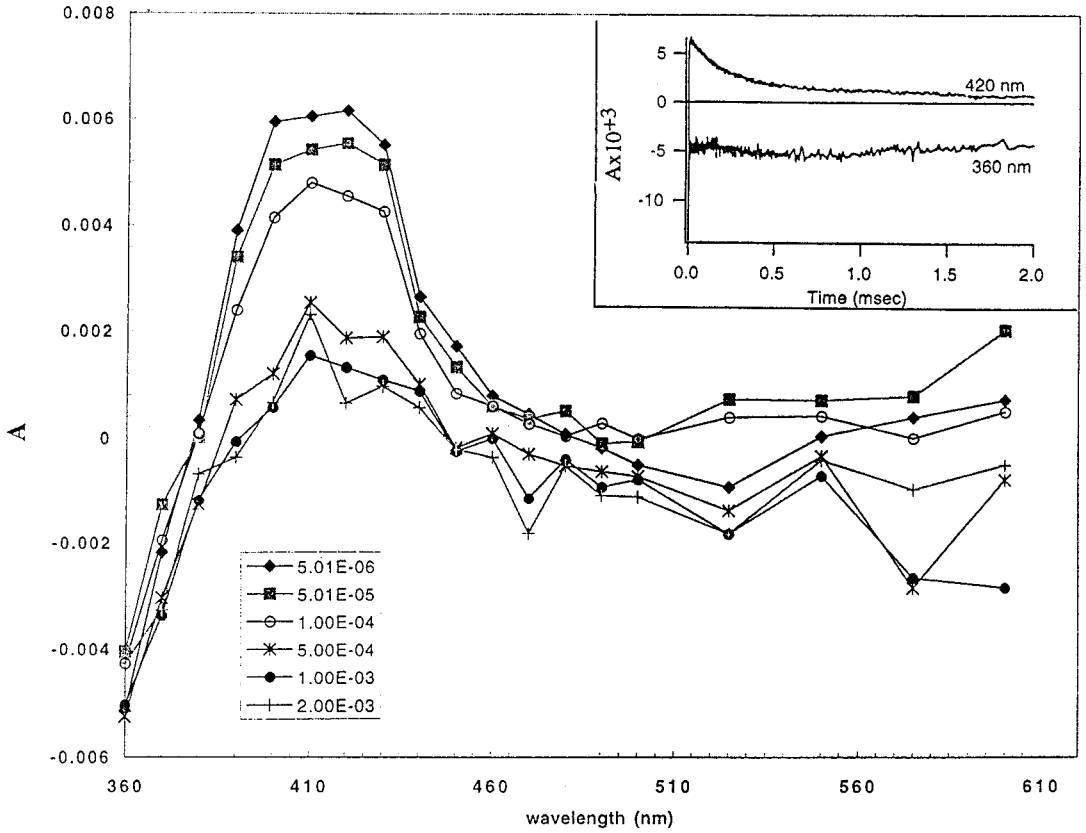

FIGURE 10. Transient absorption spectra after the laser pulse (long time domain) for solutions containing $FeCl_3$ (0.8 mM), H_2O_2 (33 mM), and XYL (12 mM) at pH 1.56. The inset shows the absorption at 420 nm and the bleaching at 360 nm.

10^{-6} M. Assuming that the decay $Cl_2^{\bullet-}$ occurred with reaction 16, an estimation of k_{16} could be made as $1/[(120 \times 10^{-6}) \cdot (4 \times 10^{-6})] = 2.1 \times 10^9$ $(M\ s)^{-1}$. This rate constant is in reasonable agreement with the published data of 3.1×10^9 $(M\ s)^{-1}$ as shown in eq 16 (Table 2).

iii. Laser Photolysis of $FeCl^{2+}$−Xylidine Solutions. Figure 8 shows the transient absorption spectra for the solutions of XYL in the presence of Fe^{3+} and Cl^- ions. The solutions containing XYL and Fe^{3+} ions were mixed immediately before the laser pulse to avoid the effect of dark reactions. Note that there is no detectable transient response due to laser photolysis of XYL in solution when Fe^{3+} ions were not added. At a decay time of 100 ns (Figure 8), an absorption band similar to the spectra shown in Figure 1 is observed corresponding to $Cl_2^{\bullet-}$ radical absorption. The inset to Figure 8 shows the rise of absorption signal reported in Figure 8 with a maximum at $\lambda = 420$ nm. This band corresponds to the aniline radical cation $[C_6H_5NH_2]^{\bullet+}$ (*35*, *36*) with a molar absorption coefficient of 4.1×10^3 $(M\ cm)^{-1}$ at $\lambda_{max} = 420$ nm. The half-width of the aniline radical cation in Figure 8 is very similar to the one reported in refs *35* and *36*. Therefore, the $XYL^{\bullet+}$ $[C_8H_9NH_2]^{\bullet+}$ radical−cation band is unambiguously assigned by pulsed laser spectroscopy.

Figure 9 presents the transient absorption spectra in the long time scale after the laser pulse for $FeCl_3$+XYL solutions. The decay of the $[C_8H_9NH_2]^{\bullet+}$ radicals up to 2 ms is reported. Photobleaching of these radicals are observed at $\lambda < 370$ nm. The bleaching originates from the reduction of the Fe^{3+} ion to Fe^{2+} ion in the presence of XYL.

The inset in Figure 9 shows the long-lived transient responsible for the photobleaching at $\lambda = 360$ nm. The decay of the $[C_8H_9NH_2]^{\bullet+}$ radicals in the inset to Figure 9 suggests radical recombination similar to the recombination of aniline radical−cations (*35*). It is difficult to determine the second-order rate constant for the reaction between these aniline radicals by optical means since the recombination products absorb in the same λ region as the radicals (*35*). The inset of Figure 9 shows that the radical recombination takes place within 2 ms. Since the radical concentration was about 3×10^{-6} M, the second-order rate constant is $2k_{17} = 10^9$ $(M\ s)^{-1}$. This value is close to the value for the recombination of aniline radical−cations in solution (*35*). It should be mentioned that aniline radical−cations recombine in the para positions. In the case of the XYL radicals, the para and the ortho positions are methyl end groups. In both cases the recombination rate constant proceed with values close to diffusion controlled rates.

iv. Laser Photolysis of Fe Salts in the Presence of H_2O_2. Fe^{3+} ions [from $Fe(ClO_4)_3$ 0.76 mM] in a solution containing NaCl (1 M) to which different concentrations of H_2O_2 were added were investigated by laser photolysis. An absorption band below $\lambda = 450$ nm was observed similar to the absorption reported in Figure 1 for $Cl_2^{\bullet-}$ in solution containing $Fe^{3+} + Cl^-$ in the absence of H_2O_2. The main difference due to the addition of H_2O_2 consisted of the temporal behavior of the transient decay. An acceleration in the transient decay was observed, indicating that $Cl_2^{\bullet-}$ reacts with H_2O_2. The reciprocal dependence of the lifetime of $Cl_2^{\bullet-}$ lifetime vs $[H_2O_2]$ concentration was plotted and a rate constant $k_{19} = (9.0 \pm 0.4) \times 10^4$ $(M\ s)^{-1}$ was found for

$$Cl_2^{\bullet-} + H_2O_2 \rightarrow H^+ + 2Cl^- + HO_2^{\bullet} \qquad (19)$$

The optical absorption changes as the H_2O_2 concentration was increased in the former Fe^{3+} solution revealed a competition between the Cl^- anion (eq 9) and H_2O_2 (eq 20) for the $Cl^{\bullet}$ in solution. Additional experimental in solutions

$$Cl^{\bullet} + H_2O_2 \rightarrow H^+ + Cl^- + HO_2^{\bullet} \qquad (20)$$

containing Cl^-, H_2O_2, and $Cl^{\bullet}$ allowed the intercept/slope

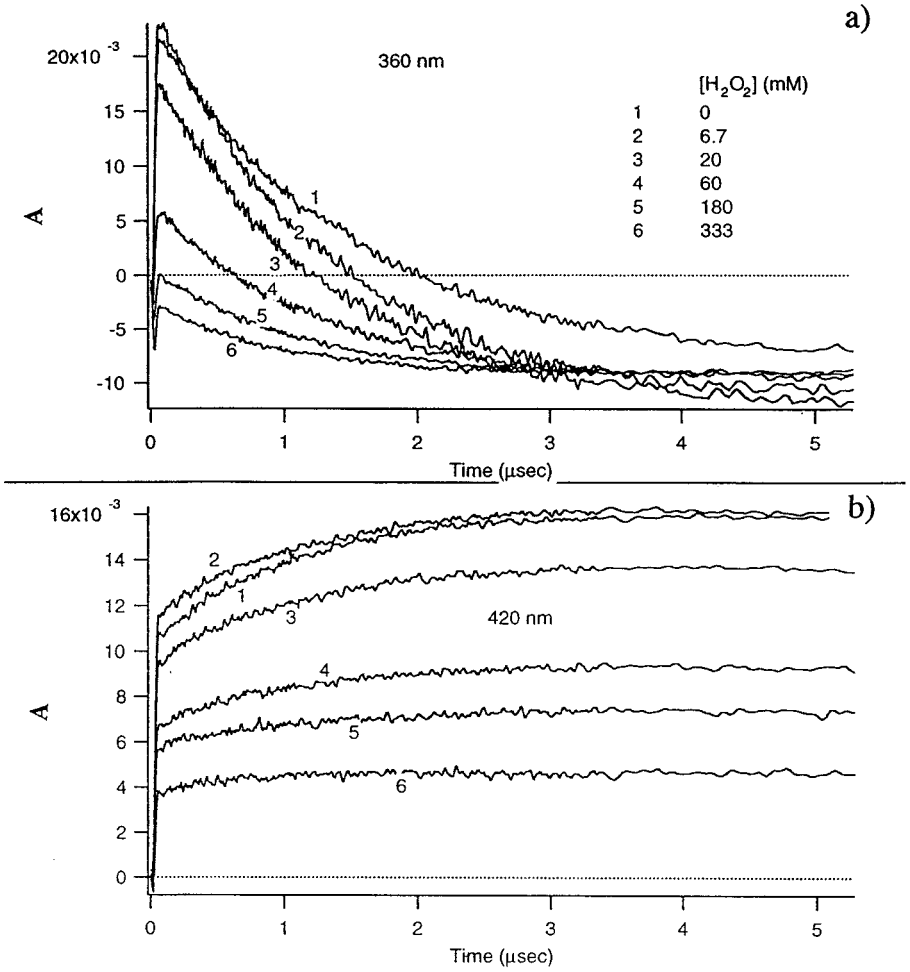

FIGURE 11. (a) The dependence of the relative optical absorption changes at 360 nm vs H_2O_2 concentrations as noted in the figure caption for the solution used in Figure 10. A short time domain was used. (b) The dependence of the transient growth in the short time domain at 420 nm for the transients in solution as a function of the added H_2O_2 concentration as noted in part a.

ratio k_{20}/k_9 [Cl^-] to be plotted and the value for k_{20} as $k_{20} = (2.8 \pm 1.0) \times 10^{10}$ $(M\ s)^{-1}$ to be determined. The acceleration in the transient decay indicates that $Cl^•$ reacts with H_2O_2.

Competitive kinetics indicated a rate constant of $k_{21} = (4 \pm 2) \times 10^{10}$ $(M\ s)^{-1}$ for the reaction of $Cl^•$ atoms with XYL (eq 21). This value coincides with the rate constant for the reaction of $Cl^•$ with aniline of 4×10^{10} $(M\ s)^{-1}$ (*39*).

$$C_8H_9NH_2 + Cl^• \rightarrow [C_8H_9NH_2]^{•+} + Cl^- \qquad (21)$$

No detailed description of these measurements are reported here since these measurements are only of marginal interest in the present study.

v. Laser Photolysis of XYL/H_2O_2/(Fe^{3+}−Cl^-) Solutions. Figure 10 shows the transient absorption spectra after the laser pulse of the ternary system XYL/H_2O_2/$FeCl_3$. These spectra with a pronounced band at ∼420 nm are similar to the bands observed in Figure 9 for solutions containing only XYL/$FeCl_3$. The main difference between the spectra reported in Figures 9 and 10 is the significantly lower intensity of the 420-nm band in the last case. This is indicative of H_2O_2 competing with the Cl^- anion and XYL for the $Cl^•$ available in the solution (see eq 20).

Figure 11a shows the decrease of the initial amplitude of the XYL^+ transient at $\lambda = 360$ nm when the concentration of H_2O_2 is increased from zero up to the relatively high concentration of 333 mM. A concomitant decrease in the magnitude of the transient growth at $\lambda = 420$ nm is observed in Figure 11b. The decay and rise time of the transient of ∼1 μs in Figure 11a,b does not change with H_2O_2 addition up to 333 mM. This is indicative of a weak interaction of the transient absorbing in solution with added H_2O_2. Knowing the rate constant of $k_{19} = 4 \times 10^4$ $(M\ s)^{-1}$ for the reaction $Cl_2^{•-}$ + H_2O_2 an estimate could be made for the characteristic reaction time reaction time of $Cl_2^{•-}$ with H_2O_2 upon addition of H_2O_2 (333 mM) of [$(333 \times 10^{-3}$ M) $(4 \times 10^4$ $M^{-1}\ s^{-1})$] ≈ 1.33×10^{-4} $s^{-1} \approx 0.76 \times 10^{-4}$ s or 76 μ for reation 19. This time is much longer than the decay time of ∼1 μs seen in Figure 11. The characteristic time of reaction is the reaction time (taken as 1/e time) for a bimolecular process Therefore, the H_2O_2 added in solution does not compete with XYL for the $Cl_2^{•-}$ radicals available in solution.

The changes in the initial amplitude of the absorbency at $t \approx 100$ ns in Figure 11a at $\lambda = 360$ nm and the decrease in the amplitude of the growth component in Figure 11b at $\lambda = 420$ nm are determined by the competitive reactions between the Cl^- anion, XYL, and H_2O_2 with $Cl^•$ atom in reactions 9, 20, and 21, respectively. The optical absorption is calculated from relations 22 and the radical concentration is stated in ref *23*:

$$A = \epsilon_{Cl_2^{•-}}[Cl_2^{•-}] + \epsilon_{XYL^•}[C_8H_9NH_2^{•+}] - \epsilon_{FeCl^{2+}}[FeCl^{2+}] \quad (22)$$

$$[Cl_2^{•-}] = \frac{k_9[Cl^-][Cl^•]_0}{k_9[Cl^-] + k_{19}[XYL] + k_{24}[H_2O_2]}$$

$$[C_8H_9NH_2^{\bullet+}] = \frac{k_{19}[XYL][Cl^{\bullet}]_0}{k_9[Cl^-] + k_{19}[XYL] + k_{24}[H_2O_2]} \quad (23)$$

The rate constant for the reaction of the $OH^{\bullet}$ radical with H_2O_2 is significantly lower than reaction 20 above with a value of $(1.7-4.7) \times 10^7$ $(M\ s)^{-1}$. The reaction of $OH^{\bullet}$ radical with H_2O_2 is more exothermic than the reaction of $Cl^{\bullet}$ atoms with H_2O_2.

$$OH^{\bullet} + H_2O_2 \rightarrow H_2O + HO_2^{\bullet} \quad (24)$$

From thermodynamic parameters (kcal/mol) for H_2O_2 (−31.47), $HO_2^{\bullet}$ (3.00), Cl^- (−31.35), $OH^{\bullet}$ (8.53), H_2O (−56.7), and Cl_2 dissolved (1.65), and the bond energy for D(Cl−Cl) = 57.1, the free energy of reactions 20 and 24 are −23.2 and −31 kcal/mol (*41*). The latter value is more exothermic by ~8 kcal/mol than the value in reaction 20. Generally, one would expect a higher rate constant for a more exothermic reaction. The nonapplicability of this rule in the case of reactions 20 and 24, for the oxidation of H_2O_2 by $OH^{\bullet}$ radicals and $Cl^{\bullet}$ atoms, could be rationalized by these reactions proceeding via a different mechanism. H atom transfer would be occurring in the case of $OH^{\bullet}$ oxidation (24) and electron transfer in the case of $Cl^{\bullet}$ oxidation (20).

In conclusion, the ferric chloride complexes have been shown to act as photoactive chromophores in photoassisted Fenton degradation of XYL. This seems also to be the case for ferric hydroxy complexes. The sequence for the reactions in the system XYL/Fe^{3+}/H_2O_2 in the presence of Cl^- anion and the rate constants for the reactions of interest are reported. Iron(III) in acid solutions show a negligibly transient signal in the absence of Cl^- anions. The $Cl_2^{\bullet-}$ radicals in solution are be formed due to the reactions of $Cl^{\bullet}$ atoms with Cl^- anion produced during the photolysis of Fe^{3+}−Cl^- complexes. These radicals can also be produced by the reaction of $OH^{\bullet}$ from $FeOH^{2+}$ with Cl^- anion. The results presented in this study have mechanistic implications for the photoassisted Fenton degradation of XYL. This will be reported in the second part of this study.

Acknowledgments

This work was supported by the Commission of the European Communities Environmental Program (Grant N° EV5V-CT 93-0249; OFES Contract N° 95 00 31, Bern).

Literature Cited

(1) Sax, N. *Dangerous Properties of Industrial Materials*; Van Nostrand and Reinhold: New York, 1984; p 3124.
(2) Papok, K. *Handbook of Motor Jets and Rocket Fuels*; Moscow, 1962; p 741.
(3) Brookes, P.; Livingston, A. *Biotech. Prog.* **1994**, *10*, 65.
(4) Helz, G.; Zepp, R.; Crosby, D. *Aquatic and Surface Chemistry*; Lewis Publishing Co.: Boca Raton, FL, 1994.
(5) Bandara, J.; Kiwi, J.; Pulgarin, P.; Pajonk, G.-M.; Albers, P. *Environ. Sci. Technol.* **1996**, *30*, 1261.
(6) Ruppert, G.; Bauer, G.; Heisler, G. *J. Photochem. Photobiol. A.* **1993**, *73*, 75.
(7) Prousek, J. *Chem. Listy* **1995**, *89*, 11.
(8) Lipchynska-Kochany, E. *Environ. Sci. Technol.* **1992**, *26*, 313.
(9) Pignatello, J. *J. Environ. Sci. Technol.* **1992**, *26*, 313.
(10) Nadtochenko, V.; Kiwi, J. *J. Chem. Soc., Faraday Trans.* **1997**, *93*, 2373.
(11) Sawyer, D. T.; Kang, C.; Llobet, A.; Redman, C. *J. Am. Chem. Soc.* **1993**, *115*, 5817.
(12) Sichev, A.; Isak, V. *Usp. Khim.* **1995**, *64*, 1183 (Russian edition).
(13) Byrne, R.; Kester, D. *J. Solution Chem.* **1978**, *7*, 373.
(14) Byrne, R.; Kester, D. *J. Solution Chem.* **1981**, *10*, 51.
(15) Evans, M. G.; Uri, N. *Nature* **1949**, *164*, 404.
(16) Evans, M. G.; Santappa, M.; Uri, N. *J. Polym. Sci.* **1951**, *7*, 243.
(17) Bates, H. G. C.; Uri, N. *J. Am. Chem. Soc.* **1953**, *75*, 2754.
(18) Saha Mukherjee, M. K.; Ghosh, A. R.; Palit, S. R. *J. Polym. Sci.* **1967**, *16*, 159.
(19) David, F.; David, P. G. *J. Phys. Chem.* **1976**, *80*, 579.
(20) David, P. G. *J. Chem. Soc., Chem. Commun.* **1972**, 1294.
(21) King, D. W.; Aldrich, R. A.; Charnecki, S. E. *Mar. Chem.* **1993**, *44*, 105.
(22) Solar, S.; Gettof, N. *Radiat. Phys. Chem.* **1986**, *28*, 229.
(23) Land, E.; Porter, G. *Trans. Faraday Soc.* **1963**, *59*, 2027.
(24) Grossweiner, L.; Joschek, H. *Adv. Chem. Ser. 50*; American Chemical Society: Washington DC, 1965; p 279.
(25) Thornton, A. T.; Laurence, G. S. *J. Chem. Soc., Dalton Trans.* **1973**, 804.
(26) Flynn, C. *Chem. Rev.* **1984**, *84*, 31.
(27) Lamb, B.; Jacques, A. *J. Am. Chem. Soc.* **1938**, *60*, 967.
(28) Rabinowitch, E.; Stockmayer, W. *J. Am. Chem. Soc.* **1942**, *64*, 335.
(29) Mulay, L.; Selwood, P. *J. Am. Chem. Soc.* **1955**, *72*, 2693.
(30) Faust, C.; Hoigne, J. *Atmos. Environ.* **1990**, *24*, 1990.
(31) Langford, H.; Carey, H. *Can. J. Chem.* **1975**, *53*, 2340.
(32) Lever, A. *J. Chem. Educ.* **1974**, *51*, 612.
(33) Balzani, V.; Carassiti, V. In *Photochemistry of Coordination Compounds*; Academic Press: London, 1970.
(34) Endicott, J. F. In *Concepts of Inorganic Photochemistry*; Adamson, A. W., Fleischauer, P. D., Eds.; p 81.
(35) Qin, L.; Tripathi, R.; Schuler, R. H. *Z. Naturforsch. A, Phys. Chem., Kosmophys.* **1985**, *40A*, 1026.
(36) Christensen, H. *Int. J. Radiat. Phys. Chem.* **1972**, *4*, 311.
(37) Jayson, G.; Parson, B.; Swallow, *J. Chem. Soc., Faraday Trans. 1* **1972**, *68*, 2053.
(38) Hasegawa, K.; Neta, P. *J. Phys. Chem.* **1978**, *82*, 854.
(39) Alfassi, Z.; Mosseri, S.; Neta, P. *J. Phys. Chem.* **1989**, *93*, 1380.
(40) Elliot, A. *Radiat. Phys. Chem.* **1989**, *34*, 753.
(41) Pourbaix, M. *Atlas of the Electrochemical Equilibria in Aqueous Solutions*; International Cebelcor: Paris, 1974.
(42) Bjergbakke, E.; Navaratnam, S.; Parsons, B. J.; Swallow, A. *J. Radiat. Phys. Chem.* **1987**, *30*, 59.
(43) Knight, R. J.; Sylva, R. *J. Inorg. Nucl. Chem.* **1975**, *37*, 779.

Received for review November 3, 1997. Revised manuscript received June 23, 1998. Accepted July 17, 1998.

ES970962E